nature plants

ARTICLES

https://doi.org/10.1038/s41477-021-00914-0

FERONIA restricts *Pseudomonas* in the rhizosphere microbiome via regulation of reactive oxygen species

Yi Song[1,2], Andrew J. Wilson[1], Xue-Cheng Zhang[3,4,8], David Thoms[1,2], Reza Sohrabi[5], Siyu Song[1], Quentin Geissmann[1,2], Yang Liu[1], Lauren Walgren[1], Sheng Yang He[5,6,7] and Cara H. Haney[1,2] ✉

Maintaining microbiome structure is critical for the health of both plants and animals. By re-screening a collection of *Arabidopsis* mutants affecting root immunity and hormone crosstalk, we identified a *FERONIA* (*FER*) receptor kinase mutant (*fer-8*) with a rhizosphere microbiome enriched in *Pseudomonas fluorescens* without phylum-level dysbiosis. Using microbiome transplant experiments, we found that the *fer-8* microbiome was beneficial. The effect of *FER* on rhizosphere pseudomonads was largely independent of its immune scaffold function, role in development and jasmonic acid autoimmunity. We found that the *fer-8* mutant has reduced basal levels of reactive oxygen species (ROS) in roots and that mutants deficient in NADPH oxidase showed elevated rhizosphere pseudomonads. The addition of RALF23 peptides, a FER ligand, was sufficient to enrich *P. fluorescens*. This work shows that FER-mediated ROS production regulates levels of beneficial pseudomonads in the rhizosphere microbiome.

Eukaryotes are associated with communities of symbiotic microorganisms (the microbiome) that affect host health and fitness[1]. In plants, the root-associated (rhizosphere) microbiome affects plant growth[2], nutrient acquisition[3] and resistance to both biotic and abiotic stresses[4–6]. While dysbiotic microbiomes have been associated with disease in both plants[7] and animals[8], in plants, enrichment of specific microbial taxa has been associated with growth promotion and pathogen protection. For instance, disease outbreaks can induce the assembly of beneficial microbes in the rhizosphere to enhance resistance to future disease[9,10]. Similarly, artificial enrichment of beneficial taxa in the laboratory or in the field can promote growth and protect plants from biotic and abiotic stresses[2,11,12]. These observations suggest that plants may be able to regulate the abundance of a few beneficial taxa to maximize fitness. However, the genetic regulators and mechanisms used by plants to control the abundance of beneficial microbes are largely unknown.

Pseudomonas fluorescens includes well-studied plant growth-promoting and biocontrol strains[13,14]. Interestingly, *P. fluorescens* and related species are routinely enriched in agricultural disease-suppressive soils. For example, disease-suppressive soils that confer resistance to *Rhizoctonia solani*[10], wheat take-all disease[15], *Fusarium* wilt[16] and black root rot[17] have all been associated with enrichment of fluorescent pseudomonads in the soil. The recurring observation that enrichment of pseudomonads is associated with pathogen protection suggests that plants may possess a mechanism to specifically regulate beneficial *Pseudomonas* species[18–20]. In addition, certain natural accessions of *Arabidopsis thaliana* support different levels of rhizosphere *Pseudomonas* species while maintaining overall highly similar microbiome compositions[21], indicating that plants may have genetic mechanisms to regulate levels of beneficial *Pseudomonas* species.

Results

***HSM13*/*FERONIA* (*FER*) inhibit rhizosphere *Pseudomonas* growth.** To identify plant genes that regulate beneficial *Pseudomonas* species levels in the rhizosphere, we made use of 16 *hormone-mediated suppression of MAMP-triggered immunity* (*hsm*) mutants identified from a previous genetic screen[22]. The *hsm* mutations affect root immunity and hormone crosstalk, and thus provide a genetic toolkit with which to identify potential new genes that shape the rhizosphere microbiome. We screened these 16 *hsm* mutants[22] for their ability to support growth of the beneficial *P. fluorescens* strain WCS365 expressing the luciferase operon (*P. fluorescens* WCS365-Luc) using a 48-well plate gnotobiotic system (Supplementary Fig. 1)[21]. We found that the *hsm13* mutant harboured consistently higher levels of rhizosphere *P. fluorescens* WCS365 (Supplementary Fig. 2).

To test whether increased levels of *P. fluorescens* in the *hsm13* rhizosphere also occur in the presence of a complex microbial community, we grew *hsm13* in natural soil (Methods and Fig. 1a) and plated rhizosphere samples (normalized to the rhizosphere weight) on King's B medium to quantify fluorescent pseudomonads[23] (Fig. 1b). We found that the fluorescent pseudomonads per gram of rhizosphere sample were enriched more than tenfold in the rhizosphere of *hsm13* relative to wild-type plants (Fig. 1b,c). We also found that *hsm13* is stunted in both natural soil and axenic plates (Fig. 1a and Supplementary Fig. 3a,b) and has a root hair elongation defect (Supplementary Fig. 3c–e). To test whether plant morphological changes affect rhizosphere pseudomonad levels, we tested

[1]Department of Microbiology and Immunology, The University of British Columbia, Vancouver, British Columbia, Canada. [2]Michael Smith Laboratories, The University of British Columbia, Vancouver, British Columbia, Canada. [3]Department of Molecular Biology, Massachusetts General Hospital, Boston, MA, USA. [4]Department of Genetics, Harvard Medical School, Boston, MA, USA. [5]Department of Energy Plant Research Laboratory, Michigan State University, East Lansing, MI, USA. [6]Department of Biology, Duke University, Durham, NC, USA. [7]Howard Hughes Medical Institute, Duke University, Durham, NC, USA. [8]Present address: DermBiont, Boston, MA, USA. ✉e-mail: cara.haney@msl.ubc.ca

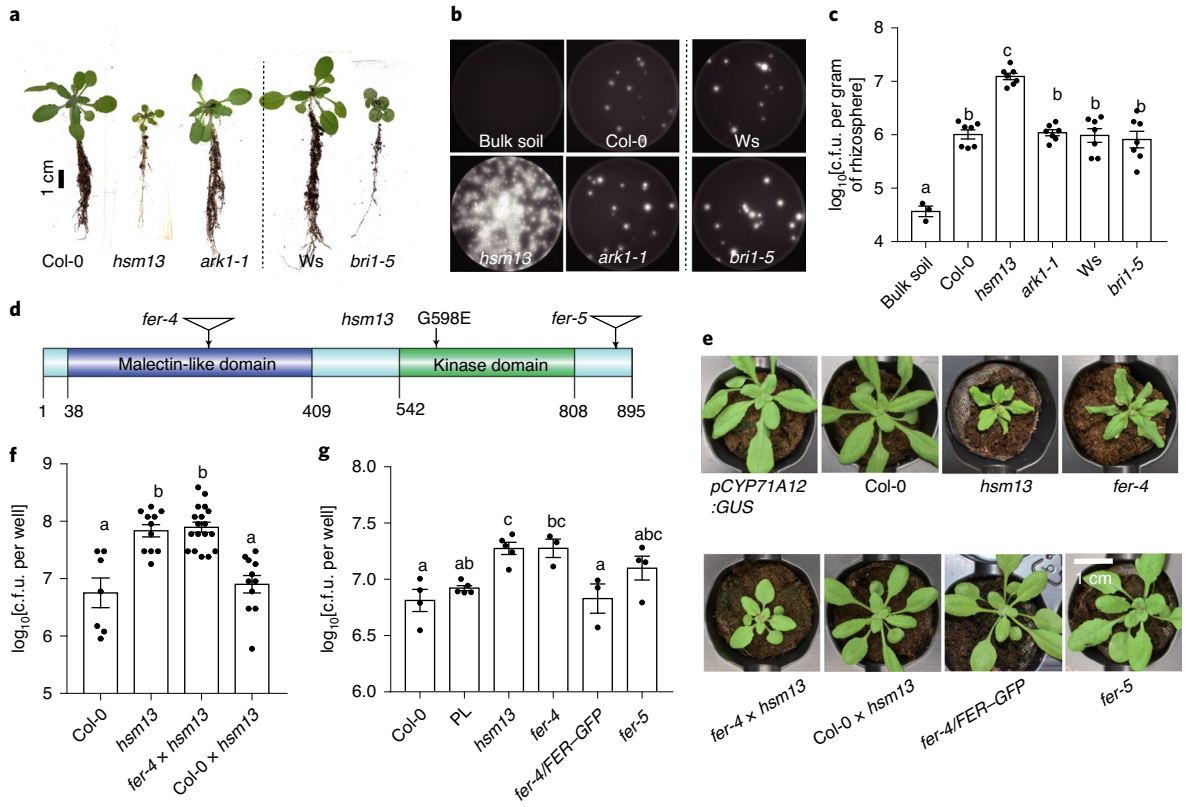

Fig. 1 | *HSM13/FER* inhibits rhizosphere *Pseudomonas* growth. a, Morphology of wild-type plants (Col-0 and Ws ecotypes) and the mutants *hsm13* and *ark1-1* (Col-0 background), as well as *bri1-5* (Ws background), when grown in natural soil. **b**, *hsm13* harboured high levels of root-associated fluorescent pseudomonads when grown in natural soil, while other mutants with similar developmental defects did not affect rhizosphere fluorescent pseudomonads levels. Rhizosphere samples were plated on King's B and imaged under ultraviolet light. **c**, Quantification of fluorescent colonies per gram of rhizosphere sample ($n = 3$ for bulk soil samples and 7 for all others). **d**, FER protein domains and insertion/mutation positions of the alleles described in this study. **e**, Phenotypes of 3-week-old wild-type plants (Col-0), the parental line (PL; *pCYP71A12:GUS*), *hsm13*, *fer-4*, *fer-5*, F1 crosses (*fer-4* × *hsm13* or Col-0 × *hsm13*) and *fer-4/FER–GFP*. **f**, F1 crosses between *fer-4* × *hsm13* had a high level of rhizosphere pseudomonads relative to Col-0, while Col-0 × *hsm13* F1s restored pseudomonads levels similar to wild-type plants ($n = 7$, 11, 17 and 11 from left to right). **g**, *fer-4* and *fer-5* mutants had elevated levels of pseudomonads in a hydroponic seedling assay. Each point represents the average of more than six plants from a single experiment. Statistical significance was determined by ANOVA and Tukey's HSD test for **c**, **f** and **g**. Different letters indicate $P < 0.05$. Means ± s.e.m. are shown.

bri1-5 (a stunted mutant unable to perceive the growth hormone brassinolide[24]; Fig. 1a) and *ark1-1* (a root hair mutant with altered microtubule dynamics[25]). We found that both *bri1-5* and *ark1-1* mutants have similar levels of rhizosphere fluorescent pseudomonads to wild-type plants (Fig. 1c), suggesting that developmental defects are unlikely to underlie the enrichment of fluorescent pseudomonads in *hsm13*.

To identify the mutation that results in enrichment of *Pseudomonas hsm13*, we crossed *hsm13* to Col-0 and performed sequencing-assisted mapping by bulk segregant analysis (Methods). We identified a genomic region with a high frequency of single-nucleotide polymorphisms (SNPs) present in the *hsm13*-like segregant population on the short arm of chromosome 3 (Supplementary Fig. 4). We identified four non-synonymous SNPs in that region, including a missense G1793A mutation in the coding sequence of *AT3G51550* (*FER*) in *hsm13* resulting in a predicted p.Gly598Glu amino acid substitution in the kinase domain (Fig. 1d). The previously described *fer-4* mutant showed a similar stunted morphology (Fig. 1e) and root hair developmental defects[26]. The F1s of a *fer-4* × *hsm13* cross had high *P. fluorescens* levels and a small plant size similar to *hsm13*, indicating that *fer-4* is allelic to *hsm13* (Fig. 1f and Supplementary Fig. 4). The F1 progeny of a Col-0 × *hsm13* cross exhibited the *P. fluorescens* levels and plant size of Col-0 plants, confirming that *hsm13* is recessive (Fig. 1f and Supplementary Fig. 4). Using the gnotobiotic system, we found that *fer-4* (CS69044) had a similarly high level of WS365-Luc to the *hsm13* mutant, and that *fer-5* (Salk_029056C) had a 1.95-fold increase in WCS365-Luc (Fig. 1g), which was consistent with previous data suggesting that *fer-5* is a partial loss-of-function allele[27]. Expression of *FER* under its native promoter (p*FER:FER–GFP*[28]) in the *fer-4* mutant completely restored the morphology and rhizosphere *P. fluorescens* WCS365 growth to wild-type levels (Fig. 1e,g). Collectively our data indicate that *hsm13* (*fer-8* hereafter) carries a loss-of-function mutation in *FER* resulting in stunting and rhizosphere pseudomonad overgrowth.

The *fer-8* microbiome is not dysbiotic. To determine the effect of the *fer-8* mutation on the overall rhizosphere microbiome composition, we grew *fer-8* and wild-type plants in the presence of natural soil microbiota (the soil was from the same site over two consecutive years: experiments 1 (Fig. 2) and 2 (Supplementary Fig. 5)) and performed 16S ribosomal RNA (rRNA)-based microbiome profiling. Samples from different years were clearly separated in the pooled principal coordinates analysis (PCoA) (Supplementary Fig. 5a), suggesting that the starting soil had the highest effect on rhizosphere microbiome composition. Despite the differences in

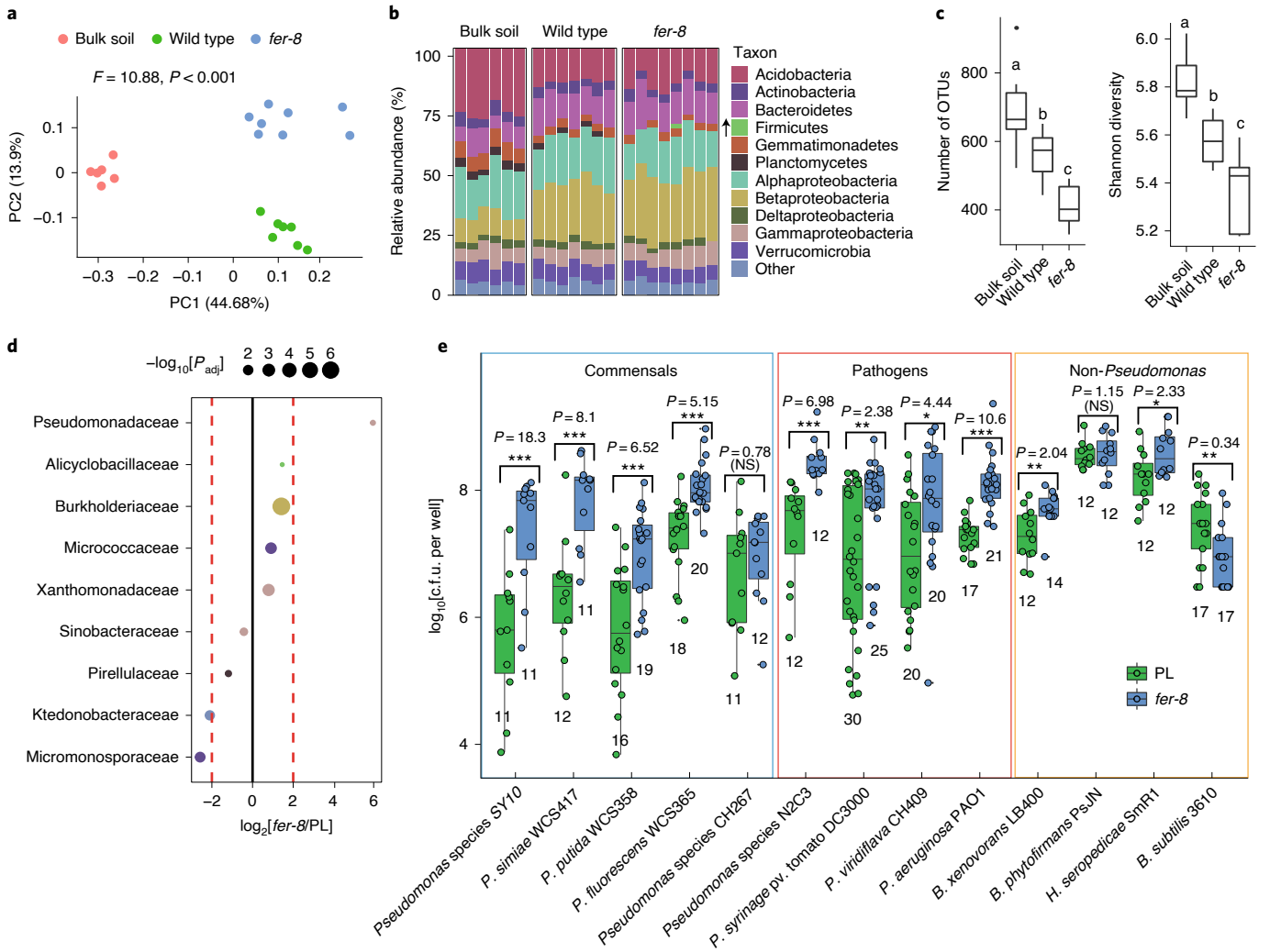

Fig. 2 | Pseudomonadaceae are enriched in the rhizosphere microbiome of *fer-8*. **a**, PCoA (based on the relative abundance of OTUs) of Bray–Curtis distances of bulk soil and rhizosphere samples of *fer-8* and the wild type (Col-0) from experiment 1. Statistical significance was calculated by permutational multivariate ANOVA ($n = 6$ for bulk soil samples and 8 for the others). **b**, Relative abundance of bacterial phyla or classes (for Proteobacteria) in bulk soil and rhizosphere samples. The arrow shows that only Firmicutes were significantly enriched in the rhizosphere of *fer-8* relative to the parental line (3.53-fold; calculated using DESeq2). **c**, Numbers of OTUs (left) and Shannon diversity indices (right) in the bulk soil and rhizosphere samples ($n = 6$ for bulk soil samples and 8 for the others). Statistical significance was determined by ANOVA with Tukey's HSD test ($P < 0.05$). Different letters indicate $P < 0.05$. **d**, Significantly differentially abundant families between *fer-8* and the wild-type parental line. The colours show the taxonomic information for each family as in the legend in **b**, and the dot sizes indicate the $-\log_{10}$-transformed adjusted P values (P_{adj}) for taxa with $P < 0.1$. The vertical red dashed lines mark a $\log_2$ fold change of 2. **e**, Quantification of individual bacterial strains grown in the rhizosphere of *fer-8* and the parental line under gnotobiotic conditions. Statistical significance of the comparison between *fer-8* and the parental line for each strain was determined by two-sided Student's *t*-test (*$P < 0.05$; **$P < 0.01$; ***$P < 0.001$). NS, not significant. The numbers denote the number of biological replicates over three independent experiments for *Pseudomonas* spp. WCS365, WCS358, DC3000, CH409 and PAO1 and two independent experiments for the others. The box plots in **c** and **e** show median values (central lines), first and third quartile (box edges) whiskers represent the range of all points excluding outliers.

soil composition from year to year, a consistently distinct microbiome composition was observed in *fer-8* relative to wild-type plants, as revealed by unconstrained PCoA, and 13.9–18.2% of the differences in samples could be explained by plant genotype (principal coordinate 2) (Fig. 2a and Supplementary Fig. 5b). We observed no consistent shift in phylum-level relative abundance between *fer-8* and wild-type plants (Fig. 2b and Supplementary Fig. 5d). The *fer-8* microbiome had lower richness (number of operational taxonomic units (OTUs)) and Shannon diversity (a metric of species richness and evenness) compared with wild-type plants (Fig. 2c and Supplementary Fig. 5c)[29]. Although several bacterial families were enriched and depleted in each experiment, only Pseudomonadaceae were enriched in both experiments (Fig. 2d and Supplementary Fig. 5e). These data indicate that the Pseudomonadaceae are robustly enriched in the *fer-8* rhizosphere microbiome without phylum-level dysbiosis.

The genus *Pseudomonas* includes both beneficial microbes and plant pathogens[30]. This raises the question of whether *fer-8* specifically enriches beneficial *Pseudomonas* species, or whether pathogenic *Pseudomonas* species are also enriched in the rhizosphere. We selected several phylogenetically diverse *Pseudomonas* strains (including both pathogens and commensal strains), along with distantly related bacterial isolates, and tested whether they are enriched in the *fer-8* rhizosphere[30]. Commensal *Pseudomonas*

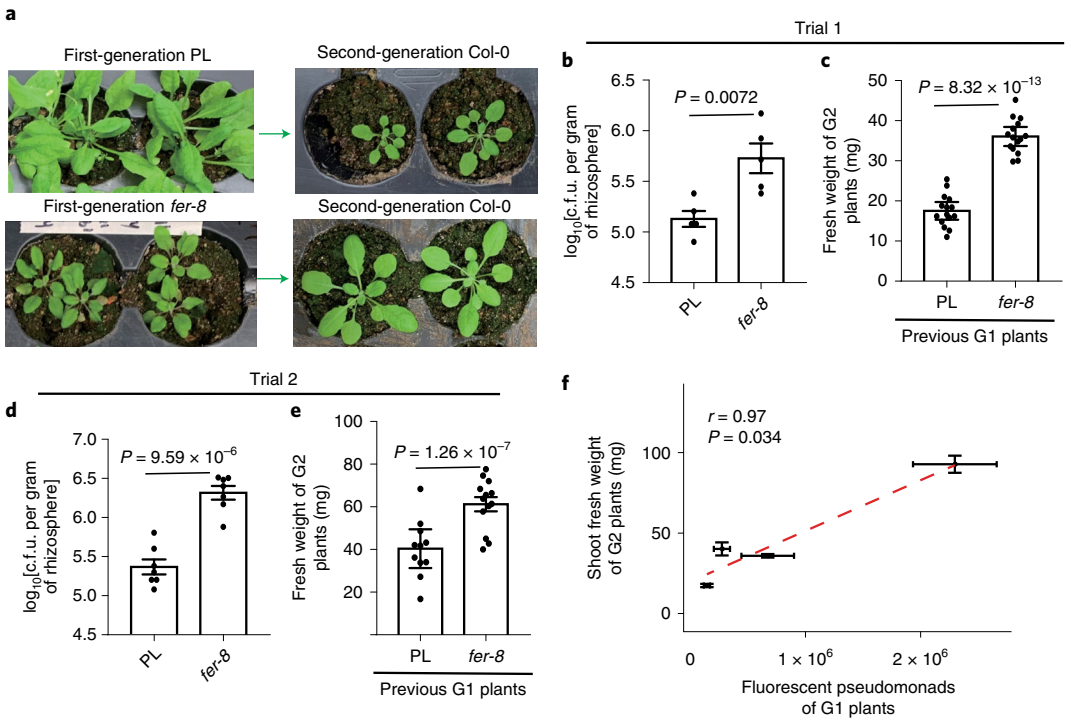

Fig. 3 | The *fer-8* microbiome is beneficial. a, Representative images of the parental line and *fer-8* grown in natural soil (generation 1), as well as wild-type Col-0 plants (generation 2). **b**, Fluorescent pseudomonads were quantified in the rhizosphere of the parental line and *fer-8* in generation 1 (G1) plants after 4 weeks of growth ($n=5$). **c**, Shoot fresh weights of G2 wild-type plants grown in the soil from microbiome transplants from parental line- or *fer-8*-cultivated soil ($n=15$). **d**,**e**, Results of a replication of the experiments shown in **b** and **c** ($n=7$ for quantified fluorescent pseudomonads (**d**); $n=11$ and 13 for shoot fresh weights of the parental line and *fer-8*, respectively (**e**)). Statistical significance was determined by two-sided Student's *t*-test in **b**–**e**, and error bars indicate ± s.e.m. **f**, Average fluorescent c.f.u. counts from the first-generation parental line and *fer-8* plants, plotted against the average shoot fresh weight of the next generation of plants grown in the same soil. The red dashed line shows the linear trend. *r* is the Pearson correlation. Statistical significance was determined by two-sided *t*-test ($t=5.26$; d.f. = 2). Each data point represents the average value of all plants from one independent experiment, and error bars indicate ± s.e.m.

strains included *P. putida* WCS358, *Pseudomonas* species CH267, *P. simiae* WCS417, *P. fluorescens* WCS365 and *Pseudomonas* species SY10 (identified from the natural soil used in this study). Pathogens or opportunistic pathogens included *P. syringae* pv. tomato DC3000, *Pseudomonas* species N2C3 (ref. [30]), *P. viridiflava* CH409 (ref. [31]) and *P. aeruginosa* PAO1. We found that eight of the nine tested *Pseudomonas* strains (with the exception of commensal strain *Pseudomonas* species CH267) were enriched between two- and 18-fold in the rhizosphere of *fer-8* relative to wild-type plants (Fig. 2e). All non-*Pseudomonas* strains tested, including *Burkholderia xenovorans* LB400, *Burkholderia phytofirmans* PsJN, *Herbaspirillum seropedicae* SmR1 and *Bacillus subtilis* 3610, exhibited twofold or lower enrichment, or were depleted, in the rhizosphere of *fer-8* (Fig. 2e). Collectively, these data suggest that the *fer-8* mutation robustly enriches most *Pseudomonas* species.

The *fer-8* microbiome is beneficial. Enrichment of fluorescent pseudomonads in the rhizosphere is reminiscent of disease-suppressive and growth-promoting soils[10,13,32]. To test whether the *fer-8*-associated microbiome is beneficial, we performed microbiome transplant experiments. We grew *fer-8* and its parental line in natural soil for 4 weeks (first generation; two plants per pot; Fig. 3a). The soil from *fer-8* or the parental line was then re-planted with wild-type plants. In the rhizosphere samples from the first-generation plants, we found enrichment of fluorescent pseudomonads in *fer-8* relative to its parental line (Fig. 3b,d). We observed a significant growth promotion effect of second-generation plants grown in the presence of a *fer-8* microbiome (Fig. 3a,c,e). Since the beneficial effects by *Pseudomonas* species have been shown to be dose dependent[33], we examined whether the growth promotion effect in the second-generation plants correlated with the abundance of fluorescent pseudomonads in soil. We found a significant positive correlation between the abundance of fluorescent pseudomonads in the rhizosphere of first-generation plants (the soil used for second-generation growth) and the biomass (shoot weight) of second-generation plants (Pearson's correlation $(r)=0.97$; $P=0.034$; Fig. 3f). These data suggest that a single mutation in *FER* shifts the soil microbiome into one that promotes growth for the next generation of plants.

In agriculture, suppressive soils are associated with enrichment of phylogenetically diverse *Pseudomonas* species. While plants might have mechanisms to specifically enrich for beneficial strains, another possibility is that, in the presence of the rhizosphere microbiome, enrichment of pathogenic *Pseudomonas* may not be harmful due to competition with commensals in the soil. *Pseudomonas* species are primarily associated with diseases of above-ground plant tissues from bacterial leaf spot to pith necrosis. However, we found that the pathogenic strains *P. syringae* pv. tomato DC3000 and *Pseudomonas* species N2C3 robustly cause stunting when added to the roots of gnotobiotic plants (Supplementary Fig. 6a,b). To test whether these strains can cause disease in soil, pathogenic *P. syringae* pv. tomato DC3000 and *Pseudomonas* species N2C3 were inoculated in the rhizosphere of plants grown in natural soil. Neither strain caused disease symptoms after inoculation to a final concentration of 10^5 and 10^6 colony-forming units (c.f.u.) per gram of soil (Supplementary Fig. 6c,d). These data suggest that enrichment of *Pseudomonas* pathogens may not efficiently cause disease in

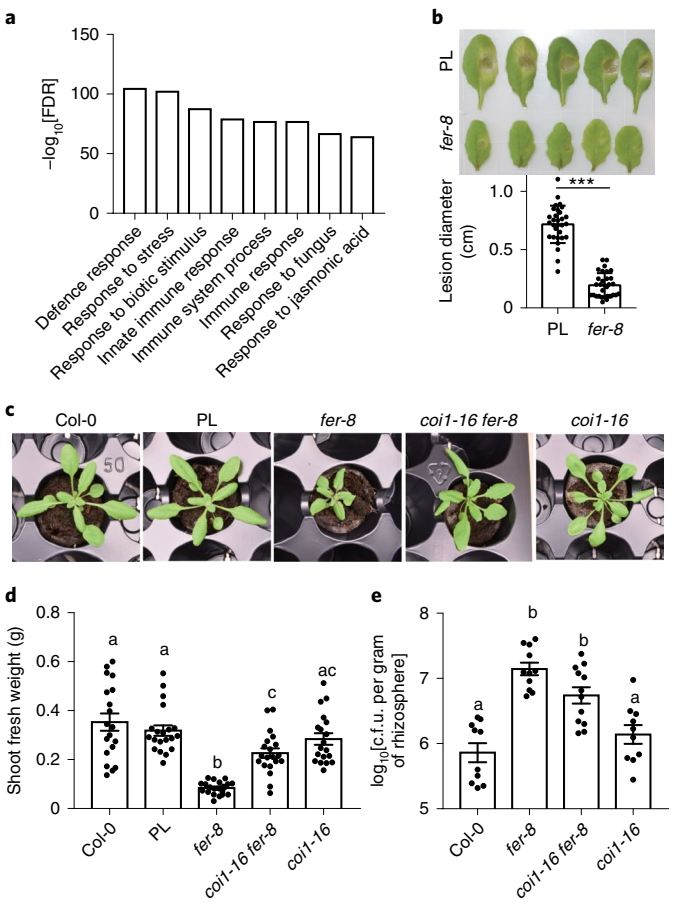

Fig. 4 | *Pseudomonas* enrichment in *fer-8* is largely independent of jasmonic acid signalling. a, Selected Gene Ontology categories from the top 20 significantly enriched Gene Ontology terms of differentially expressed genes in *fer-8* relative to the parental line in leaves (based on the −log-transformed false discovery rate (FDR) values). Gene Ontology enrichment analysis was performed using AgriGO. **b**, *fer-8* is resistant to the necrotrophic pathogen *B. cinerea*. The image shows the lesion size 3 d after inoculation ($n = 30$ and 31 for the parental line and *fer-8*, respectively; two independent experiments). The data represent means ± s.e.m. Statistical significance was determined by two-sided Student's *t*-test ($P = 6.08 \times 10^{-22}$; ***$P < 0.001$). **c**, Growth phenotypes of Col-0, the parental line, *fer-8*, *coi1-16 fer-8* and *coi1-16*. The images were taken 3 weeks after germination. **d**, Quantification of the shoot fresh weights of different genotypes 3 weeks after germination ($n = 14$, 20, 20, 20 and 19 from left to right). The data are from two independent experiments. **e**, A *fer-8 coi1-16* double mutant does not restore the *Pseudomonas* overgrowth phenotype in *fer-8* ($n = 10$, 11, 12 and 10 from left to right). The data are from three independent experiments. For **d** and **e**, the data show means ± s.e.m. and different letters indicate $P < 0.05$, as determined by ANOVA with Tukey's HSD test.

the presence of a natural soil community, so general enrichment of rhizosphere *Pseudomonas* might not present a risk of disease.

***Pseudomonas* enrichment in *fer-8* is largely independent of jasmonic acid signalling.** To reveal transcriptional changes in the *fer-8* mutant that might explain the increase in *Pseudomonas* colonization, we performed transcriptional profiling in both shoots and roots from *fer-8* and the parental line (Supplementary Table 1). We identified 675 upregulated genes in the shoots of *fer-8* relative to wild-type plants (Supplementary Table 2). Surprisingly, we found only 82 upregulated genes in *fer-8* roots relative to the parental line, and there were no significantly enriched Gene Ontology terms. In contrast, we found that the genes upregulated in shoots were enriched in Gene Ontology terms related to defence, response to fungi and jasmonic acid signalling (Fig. 4a and Supplementary Table 3), consistent with previous reports of jasmonic acid activation in the shoots of *fer-4* (ref. [26]). The *fer-8* mutant exhibited enhanced resistance to the fungal pathogen *Botrytis cinerea* and shoot-specific expression of jasmonic acid-responsive genes (Fig. 4b and Supplementary Fig. 7). The transcriptional changes in shoots were largely limited to jasmonic acid signalling, while the expression of other hormone signalling pathways was relatively similar between *fer-8* and the parental line (Supplementary Fig. 7 and Supplementary Table 4). These data suggest that the *fer-8* mutation results in activation of jasmonic acid signalling in shoots but not roots.

While we did not observe strong activation of jasmonic acid signalling in the root transcriptome, we hypothesized that a shoot-to-root jasmonic acid-dependent signal could affect the rhizosphere microbiome. To test whether jasmonic acid-mediated autoimmunity in shoots affects rhizosphere *Pseudomonas* colonization in *fer-8*, we constructed a double mutant of *coi1-16* (deficient in jasmonic acid perception[34]) and *fer-8* (*coi1-16 fer-8*). We found that the *coi1-16 fer-8* mutant suppressed the stunting phenotype of *fer-8*, suggesting that the stunting phenotype in *fer-8* is caused by shoot jasmonic acid autoimmunity similar to the recent report in a *fer-4* mutant[35] (Fig. 4c,d). However, the *coi1-16 fer-8* double mutant retained high *Pseudomonas* levels that were not significantly different from the *fer-8* single mutant (Fig. 4e). Enhanced jasmonic acid in shoots might antagonize salicylic acid signalling[36]. To determine whether the effects on salicylic acid signalling could explain the enhanced levels of *P. fluorescens* in the *fer-8* mutant, we tested rhizosphere *Pseudomonas* levels in the salicylic acid perception-deficient mutant (*npr1-1*)[37], the salicylic acid biosynthesis mutant (*sid2-1*)[38] and the salicylic acid autoimmune mutant (*snc1*)[39]. We found no significant changes in rhizosphere fluorescent pseudomonads in salicylic acid mutants (Supplementary Fig. 8). These data collectively indicate that neither jasmonic acid autoimmunity nor salicylic acid–jasmonic acid antagonism fully explains the increase in rhizosphere *Pseudomonas* colonization in the *fer-8* mutant.

FER regulates root reactive oxygen species (ROS) to control pseudomonads. FER regulates both the microbe-associated molecular pattern (MAMP)-triggered ROS burst (inducible ROS)[40] and basal ROS levels in roots through Rho of plants 2 (ROP2; a small GTPase)[28]. We hypothesized that loss of FER might decrease basal or inducible ROS, resulting in *Pseudomonas* overgrowth. By staining roots with the ROS-sensitive dye 2′,7′-dichlorodihydrofluorescein diacetate (H_2DCFDA)[28], we found a significant decrease in basal ROS levels in buffer-treated *fer-8* compared with the parental line (Fig. 5a,b). Importantly, roots treated with *P. fluorescens* WCS365 exhibited a significant reduction in root ROS levels in both *fer-8* and the parental line (Fig. 5a,b), indicating that suppression of basal root-surface ROS might be crucial for *Pseudomonas* fitness in the rhizosphere. To test whether altering rhizosphere ROS levels could affect *Pseudomonas* growth in the rhizosphere, we tested *respiratory burst oxidase homologue* mutants (*rbohD* and *rbohF*), which are deficient in NADPH oxidase and dampen apoplastic ROS production[41]. We found that both *rbohD* and *rbohF* have significantly elevated rhizosphere fluorescent pseudomonads in natural soil (Fig. 5c).

FER interacts with immune receptors and facilitates the complex formation of innate immune receptor complexes that include EF-TU RECEPTOR (EFR) and FLAGELLIN-SENSING 2 (FLS2), with their co-receptor BRASSINOSTEROID INSENSITIVE 1-ASSOCIATED KINASE 1 (BAK1)[40]. We reasoned that if FER

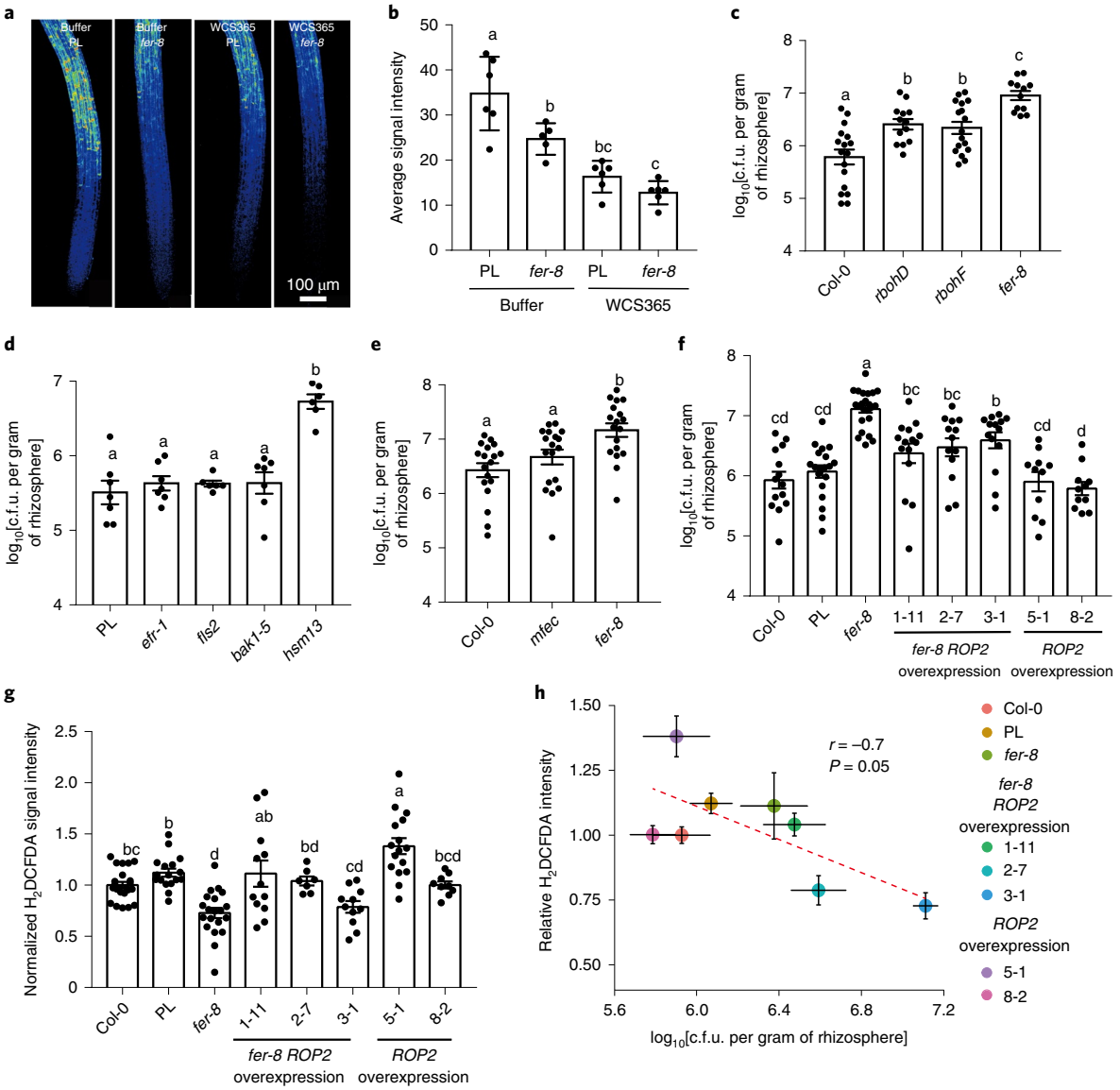

Fig. 5 | FER regulates root ROS to control pseudomonads. a, Representative images of H_2DCFDA-stained roots of the parental line and *fer-8* pre-treated with buffer or *P. fluorescens* WCS365. Representative images from one experiment are shown, repeated twice with consistent results. **b**, Quantified average H_2DCFDA signal intensity in the roots (two independent experiments). **c**, Mutants deficient in NADPH oxidase (*rbohD/F*) showed elevated rhizosphere fluorescent pseudomonads when grown in soil ($n = 17$, 13, 17 and 12 from left to right; three or four independent experiments). **d**, Mutants deficient in immune receptors that are interaction partners of FER (*fls2*, *efr-1* and *bak1-5*) did not affect rhizosphere *Pseudomonas* levels ($n = 7$, 7, 6, 7 and 6 from left to right). **e**, The quadruple mutant *mfec* does not change rhizosphere pseudomonad levels as *fer-8* does ($n = 18$ from three independent experiments). **f**, Overexpression of *ROP2* (a positive regulator of NADPH oxidase) in *fer-8* decreases rhizosphere levels of fluorescent pseudomonads ($n = 14$, 19, 25, 15, 13, 14, 11 and 11 from left to right; three to five independent experiments). **g**, Relative signal intensity values of root H_2DCFDA staining for Col-0, the parental line, *fer-8*, *fer-8 ROP2* overexpression (lines 1-11, 2-7 and 3-1) and *ROP2* overexpression (lines 8-2 and 5-1) ($n = 23$, 17, 20, 12, 7, 11, 16 and 9 from left to right; two to four independent experiments). Data from different independent experiments were normalized to the average values of the Col-0 control from the same experiment. **h**, Average $\log_{10}$[fluorescent c.f.u. per gram of rhizosphere] from different genotypes, plotted against the average relative H_2DCFDA stain signal intensity. A linear trend is shown by the red dashed line. *r* is the Pearson correlation. Statistical significance was determined by two-sided *t*-test ($t = -2.4$; d.f. = 6). In **b**–**g**, different letters indicate $P < 0.05$, as determined by ANOVA with Tukey's HSD test.

regulates pseudomonads through its immune scaffold function, immune receptor mutants should also increase rhizosphere pseudomonads. However, we found that *fls2*, *efr-1* and *bak1-5* mutants all have similar levels of rhizosphere fluorescent pseudomonads to wild-type plants when grown in natural soil (Fig. 5d). BAK1 (also known as SERK3) belongs to the SOMATIC EMBRYOGENESIS RECEPTOR KINASE (SERK) family and is partially redundant with SERK4 (also named BKK1) in immune signalling[42]. We found that the *bak1-5 bkk1-1* double mutant[43] did not affect rhizosphere *Pseudomonas* levels in natural soil (Supplementary Fig. 9), suggesting that FER interactions with BAK1/BKK1 are largely dispensable for regulating rhizosphere *Pseudomonas* levels. A recent study found that a mutant deficient in multiple immune receptors and vesicle trafficking (*min7 fls2 efr cerk1* (*mfec*)) causes dysbiosis in the endophytic phyllosphere microbiome and decreased alpha diversity[7]. We wondered whether the *mfec* mutant would show rhizosphere enrichment of *Pseudomonas* similar to *fer-8*. Although the enrichment of pseudomonads in *fer-8* was reproducible in a distinct

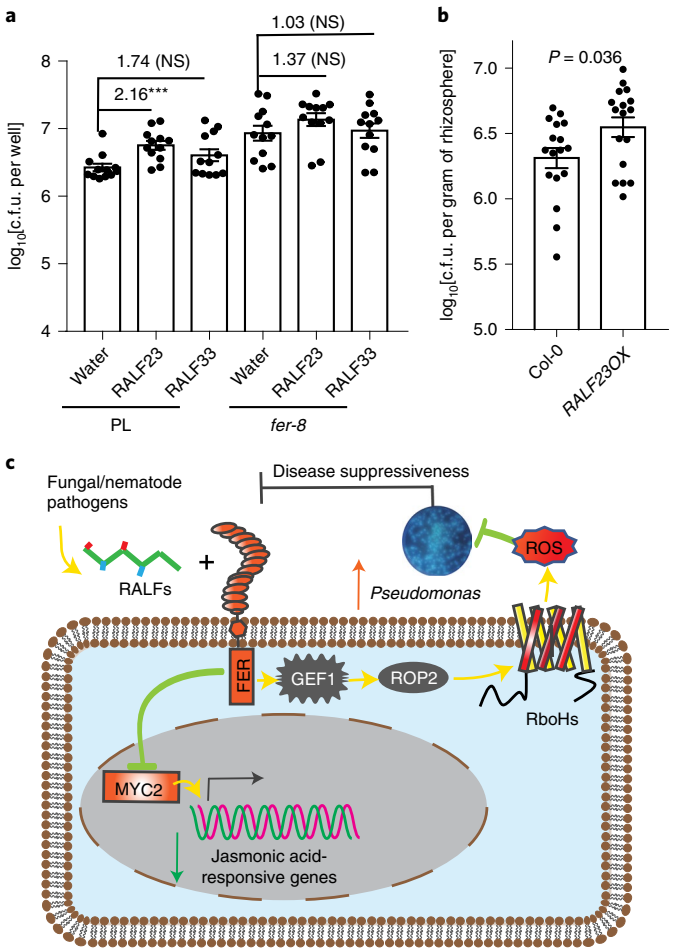

Fig. 6 | RALF enriches *Pseudomonas* levels in the rhizosphere. a, Treatment with RALF peptides enriched rhizosphere *P. fluorescens* WCS365-Luc in the parental line but not in *fer-8*. The numbers above each bar represent the fold change of each treatment compared with the water-treated control. The data were obtained from two independent experiments ($n=12$). **b**, *RALF23* overexpression showed enriched fluorescent pseudomonads in natural soil ($n=17$ from three independent experiments). Statistical significance in **a** and **b** was determined by two-sided Student's *t*-test; ***$P<0.001$. The data represent means ± s.e.m. **c**, A proposed model of FER-dependent enrichment of fluorescent pseudomonads based on this and previous work. Fungal and nematode pathogens can secrete RALF-like peptides to hijack FER and suppress jasmonic acid signalling. The FER ligand RALF negatively regulates jasmonic acid signalling through repression of MYC2, and enhances *Pseudomonas* levels through activation of guanine nucleotide exchange factor 1 (GEF1), ROP2 and RBOHs.

natural soil (from Michigan State, United States), we did not observe significant enrichment of pseudomonads in the rhizosphere of *mfec* mutants (Fig. 5e). This indicated that the mechanism of rhizosphere microbiome changes in *fer-8* is distinct from the *mfec* mutant.

FER positively regulates ROP2 activity, which is a positive regulator of plasma membrane NADPH oxidases, and *fer-4* and *fer-5* mutants have reduced basal ROS levels in roots[28]. To test whether *FER* acts through NADPH oxidase to regulate rhizosphere *Pseudomonas*, we overexpressed *ROP2* in *fer-8*, which has previously been shown to enhance root ROS in a *fer-5* mutant[28]. We found that *fer-8 ROP2OX* significantly decreased the numbers of fluorescent pseudomonads observed in the *fer-8* rhizosphere (Fig. 5f) and increased root ROS levels relative to *fer-8* (Fig. 5g). By plotting average rhizosphere fluorescent pseudomonad levels against average ROS levels (as measured by H_2DCFDA signal intensity) in different genetic backgrounds, we saw a significant negative correlation ($r=-0.7$; $P=0.05$) between ROS and pseudomonad levels (Fig. 5h). We reasoned that if RBOH-mediated ROS production is responsible for the relatively specific enrichment of *Pseudomonas*, the *rboh* mutants should also show similarly specific enrichment of *Pseudomonas* strains in the rhizosphere. We found that the *rbohF* mutant enriches (4- to 14-fold) *Pseudomonas* pathogens and commensals (except for *Pseudomonas* species CH267), but not non-*Pseudomonas* strains (Supplementary Fig. 10). Collectively, these data indicate that *ROP2*-mediated regulation of ROS is required for *FER*-mediated regulation of rhizosphere *Pseudomonas* growth.

RALF23 perception by FER enriches *Pseudomonas* colonization. FER is the receptor for many RALF peptides, including RALF23, which negatively regulates FER function[40,44,45]. Both the fungal pathogen *Fusarium oxysporum* and nematodes secrete RALF-like peptides to manipulate FER activity and suppress jasmonic acid signalling, thus promoting pathogenesis[46–48]. RALF23 shares high sequence similarity with nematode-secreted MiRALF1 and MiRALF3 (ref. [47]). We treated plants with RALF23 and its relative RALF33 peptides in the gnotobiotic system and found that synthetic RALF23 treatment (1 μM) causes significant enrichment of *P. fluorescens* WCS365 growth in the wild-type but not the *fer-8* rhizosphere (Fig. 6a). We also found that the *RALF23* overexpression line has significantly higher levels of fluorescent pseudomonads in natural soil relative to wild-type plants (Fig. 6b). Root-associated *Pseudomonas* species are enriched in disease-suppressive soil towards either *F. oxysporum* or nematodes[16,49], suggesting that RALF–FER signalling is a possible mechanism for increased *Pseudomonas* after pathogen attack (Fig. 6c).

Discussion

In this study, we found that loss of *FER* receptor-like kinase robustly enriches *Pseudomonas* in the rhizosphere. Although emergent evidence shows that changes in root exudate composition affect microbiome structure[50,51], we found that *FER*-regulated basal ROS production through ROP2-dependent NADPH oxidase activity is a new mechanism required for the negative regulation of rhizosphere *Pseudomonas*. Although the ROS burst is a critical step of innate immune activation in plants, we found that FER-mediated regulation of rhizosphere pseudomonads is dependent on basal ROS rather than inducible ROS triggered by MAMP perception and innate immune receptors. From an evolutionary standpoint, this could be because roots are constitutively exposed to a MAMP-rich environment and are less sensitive to MAMPs[52]. Moreover, many rhizosphere microbes can suppress pattern-triggered immunity[53] and thus plants may rely on basal ROS levels to gate rhizosphere *Pseudomonas* colonization.

It is unclear why decreased ROS in *fer-8* relatively specifically enriches *Pseudomonas* species as ROS is toxic to most microbes. We speculate that root-surface ROS only affects a localized region close to the root surface (the rhizoplane), which may be a region where beneficial *Pseudomonas* species are specifically enriched[21], and therefore may be more vulnerable to plant defences than other taxa. Spatial–temporal resolution of rhizosphere communities may reveal why manipulation of root ROS effectively gates colonization by *Pseudomonas* species.

FER is a versatile receptor kinase that regulates growth and immunity and is widely present in crops[54], and RALF genes have been identified from 51 different plant species[55]. Both fungal pathogens and nematodes secrete RALF-like peptides to hijack FER signalling[46–48], suggesting that the RALF–FER pathway is an evolutionarily conserved molecular target for pathogens. Guarding FER by recruiting beneficial *Pseudomonas* may be a way for plants

to recruit beneficial microbiota in the face of pathogen attack. Collectively, this work suggests that plants can use a single regulator and simple liner pathway to enrich beneficial *Pseudomonas* in the complex rhizosphere microbiome, and has the potential to guide new breeding and microbiome engineering practices in agriculture.

Methods

Plant materials and growth methods. *Arabidopsis* seeds were surface sterilized (washed in 70% ethanol for 2 min, 10% bleach for 2 min and three times in sterile water) and stored at 4 °C for at least 2 d before use. For assays on plates with solid media, seedlings were grown on 1/2× MS medium with 1% phytoagar and 1% sucrose. Plates were grown at 22 °C under 90–100 µE light on a 12 h light/12 h dark cycle. The *Arabidopsis* Col-0 ecotype was used as the wild-type genetic background in this work, and *fls2* (ref. [56]), *efr-1* (ref. [57]), *bak1-5* (ref. [43]), the *bak1-5 bkk1-1* double mutant[43], *mfec*[7] and *RALF23* overexpression[58] were reported previously. The *ark1-1* mutant has a 35Spro:*EB1b*-GFP reporter, which does not alter the root hair phenotype[25].

Gnotobiotic rhizosphere bacterial quantification assay. The assay (Supplementary Fig. 1) was performed as described previously[21]. Briefly, seeds were germinated on Teflon mesh discs in 300 µl MS media with 2% sucrose in 48-well plates. After 10 d, the media was changed to 270 µl media without sucrose (1× MS and 0.1% MES buffer) so that bacteria relied on plant root exudate as a carbon source. After two more days, 30 µl *P. fluorescens* WCS365, transformed with the LUX operon from *Aliivibrio fisheri* (WCS365-Luc hereafter), was added. Two days after inoculation, media containing bacteria from the rhizosphere in 48-well plates was transferred to opaque white 96-well plates before reading to avoid background from the plants and Teflon mesh, and Luc photo counts were measured using a SpectraMax i3 plate reader (Molecular Devices). Any plants with translucent or water-soaked leaves were discarded from the assay and not used for bacterial treatment. To generate WCS365-Luc, a transposon containing the *A. fisheri* LUX operon was integrated into the *P. fluorescens* WCS365 genome by conjugation with *Escherichia coli SM10λpir* containing pUT-EM7-LUX[59]. To ensure that the insertion did not affect WCS365 growth promotion ability, we confirmed that WCS365-Luc promoted lateral root growth to a similar level as wild-type WCS365 (Supplementary Fig. 1). We found a linear relationship between the WCS365-Luc bacterial c.f.u. counts and the luciferase signal (Supplementary Fig. 1), indicating that the WCS365-Luc strain can be used to approximate bacterial numbers in the rhizosphere.

For RALF treatments in 48-well plates, RALF23 and RALF33 peptides were synthesized by EZBiolab and dissolved in water. Peptides were added to a final concentration of 1 µM at the same time as bacterial inoculation. Then, c.f.u. counts were estimated (based on the WCS365-Luc photo counts measured using a plate reader 3 d after inoculation) using a standard curve.

Mapping of *hsm13*. The *FER* gene was cloned by bulk segregant analysis[60]. We hypothesized that the same mutation might cause both stunting and rhizosphere *Pseudomonas* enrichment in *hsm13*, so we used stunting to screen for *hsm13*-like segregants. Briefly, we backcrossed *hsm13* to wild-type plants (Col-0) and identified 30 stunted F2 segregates (*hsm13* like) from 140 F2 plants. We found that all F3s from these lines were stunted, indicating that they were homozygous for the mutation leading to stunting. We then sampled 90 plants (three plants from each F2 line; one leaf per plant) and extracted DNA from each leaf separately. Genomic DNA samples were quantified using Quant-iT PicoGreen dsDNA Reagent (Invitrogen). DNA from different samples was mixed at equimolar ratios. A 1:1 mix of DNA from Col-0 and *pCYP71A12:GUS* (the parental line of *hsm13*) was also sequenced as a reference sample. Paired-end sequencing (150 base pair (bp) reads) was performed on an Illumina HiSeq by Novogene. After filtering, approximately 35 million single-end reads (approximately 37× coverage after trimming, mapping and filtering) and 34 million single-end reads (approximately 37× coverage) were mapped to the TAIR10 *Arabidopsis* reference genome for the *hsm13* segregate population and pooled reference samples, respectively[61]. After SNP calling relative to the TAIR10 reference genome, 333 and 486 non-synonymous SNPs were identified in the *hsm13* segregates and pooled reference samples, respectively. P_{SNP} was calculated as mutant SNP/(mutant SNP + wild-type SNP) in Excel. SNPs present in both *hsm13* segregates and the pooled reference samples were discarded from further analysis.

Harvesting rhizosphere samples. Natural soil for the majority of experiments (except Fig. 5e) was harvested from the UBC Farm (49° 15.0′ N, 123° 14.4′ W), Vancouver, British Columbia, Canada. This is a disturbed site that was naturally colonized by wild *A. thaliana*. The top 10–20 cm of soil was collected and sieved (using a 3-mm sieve) to remove rocks, insects and plant debris. *Arabidopsis* seedlings were grown on 1/2× MS plates with 1% sucrose for 8–10 d before transplanting to soil. We blended additional inorganic growth materials and soils to improve drainage and plant health. The final soil substrate consisted of 1:0.5:1 natural soil:calcinated clay (Turface):perlite for microbiome sequencing and other studies using natural soil. Both rhizosphere and bulk soil samples were harvested 17–20 d after transplanting.

The experiment to quantify fluorescent *Pseudomonas* in the rhizosphere of *fer-8* and *mfec* (Fig. 5e) was performed in natural soil collected in Michigan, United States. Plants were grown in *Arabidopsis* Mix greenhouse potting soil (equal parts of Suremix (Michigan Grower Products), medium vermiculate and perlite), which was autoclaved once before use. Individual pots were supplemented with natural soil slurry prepared from a soil in which wild accessions of *Arabidopsis* were found at Michigan State University's Southwest Michigan Research and Extension Center (Benton Harbor). To prepare the soil slurry, 25 g of the soil was mixed with 1 l of autoclaved double-distilled water for 30 min on an orbital shaker and filtered through a 70-µm cell strainer. Then, 20 ml soil slurry was supplemented to each pot uniformly by top irrigation. Plants were grown under a relative humidity set at 50%, a temperature of 22 °C, a light intensity of 100 µE m^{-2} s^{-1} and a photoperiod of 12 h light:12 h dark. Four-week-old plants were used for rhizosphere sampling based on the protocol below.

To collect rhizosphere samples, we collected roots and closely adhered soil. To harvest rhizosphere samples, pots were inverted to transfer the soil and whole plant to a gloved hand. The soil was then gently loosened from the root until just the roots and closely adhered soil remained. Gloves were cleaned with 70% ethanol between samples and fresh gloves were used between genotypes. Rhizosphere samples were weighed and buffer was added to 0.05 g ml^{-1} (7.5 mM $MgSO_4$ and 20% glycerol). Samples were homogenized using a TissueLyser (2 × 90 s at 25 Hertz). Samples were serially diluted and 100 µl of the bulk soil (0.0025 g ml^{-1}) or rhizosphere sample (0.00025 g ml^{-1}) was plated on King's B plates and imaged using an ultraviolet light source.

Rhizosphere microbiome transplant assay. For microbiome transplant experiments, we grew first-generation plants (either *fer-8* or the parental line) for 3.5–4 weeks (two plants per pot) in natural soil to allow assembly of a genotype-specific rhizosphere microbiome. We then cut the shoots of the first-generation plants and thoroughly mixed all soil from the same genotype together in a sterilized container. We then immediately (the same day) put the mixed soil (with genotype-specific microbiomes) into new clean pots to grow second-generation plants. The trays and growth chamber were sterilized with 70% ethanol before the experiment and all plants were watered with autoclaved water for both the first- and second-generation plants. Different genotypes were put in separate trays side by side in the same growth chamber and grown under 80–100 µE light on a 12 h light/12 h dark cycle. For first-generation plants, about 15% of the plants were bolting 4 weeks after transplanting. We only chose non-bolting plants for the rhizosphere sampling to avoid the effects of differences in developmental stage. For both first- and second-generation plants, 1 l of 1/4× Hoagland's fertilizer was added to each tray.

16S rRNA microbiome sample preparation, sequencing and analysis. For microbiome sequencing, four individual rhizosphere or bulk soil samples were pooled as one replicate. Sample processing and sequencing were performed as described in the Earth Microbiome Project Illumina 16S rRNA protocol[62]. Briefly, total soil or rhizosphere DNA was extracted using the PowerSoil DNA Isolation kit (Mo Bio Laboratories). DNA concentrations were determined using a Quant-iT PicoGreen dsDNA Assay Kit. Paired-end 300-bp sequencing was performed on an Illumina MiSeq. Adaptor sequences were trimmed with cutadapt, and DADA2 was used to generate an amplicon sequence variant table[63]. The Qiime2 implementation of vsearch was used to bin amplicon sequence variants at 97% identity, and the q2-feature-classifier was used to assign taxonomy using a naive Bayesian approach. Principle covariate analysis was performed using Bray–Curtis dissimilarity of relative abundances (OTU level) with the vegan package in R. Differentially abundant families were identified using the DESeq2 package[64].

Transgenic plants. To overexpress *ROP2*, a gene-specific primer pair was used to amplify the coding sequence of *ROP2* (forward: 5′-ATA**TCTAGA**ATGGCGT CAAGGTTTATAAAGT-3′; reverse: 5′-ATA**CTGCAG**TCACAAGAACGCGCA ACGGTTC-3′), with the restriction enzyme sites for *Xba*1 and *Pst*1 (shown in bold) added to the forward and reverse primers, respectively. The PCR product was digested by *Xba*1 and *Pst*1 enzymes and subcloned into a binary vector, pCambia1300 (ref. [65]). The sequence was confirmed by Sanger sequencing and the plasmid was introduced into *Agrobacterium* GV3101 for floral dip transformation of *Arabidopsis* (Col-0 and *fer-8*). T1 and T2 transformants were selected and confirmed in 1/2× MS with 1% sucrose and 50 µg ml^{-1} hygromycin.

Plant genotyping. The primers for *fer-4* were as follows[27]: P1 (5′-GATTACTCT CCAACAGAGAAAATCCT-3′); P2 (5′-CGTATTGCTTTTCGATTTCCTA-3′); P3 (5′-ACGGTCTCAACGCTACCAAC-3′); and P4 (5′-TTTCCCGCCTTCGG TTTA-3′). The primers for Salk_029056C were as follows: LP (5′-TGGTAGGATT CCGTTAAAATGC-3′); RP (5′-CAGAGTATTTCAGACGGCAGC-3′); and LB (5′-ATTTTGCCGATTTCGGAAC-3′). For the detection of *ROP2OX* in T1 lines, we used a pair of primers targeting the 35S promoter and *ROP2* gene (5′-CTAT CCTTCGCAAGACCCTTC-3′ and 5′-GCAACGGTTCTTATTCTTTTTCT-3′, respectively).

For the *fer-8 coi1-16* double mutant, F2 progeny of *fer-8* × *coi1-16* were selected on 1/2× MS agar plates supplemented with 20 µM MeJA. Seedlings insensitive

to jasmonic acid-mediated root growth inhibition were selected as *coi1-16* homozygous lines, and *fer-8* allele-specific SNP detection primers were designed using a web tool[66]. The primer (5′-ACATCGTCATCTTGTGTCCTTGATGGG -3′ and 5′-GGGTTCAAGGCTGGACGAGCG-3′) can specifically amplify the wild-type *FER* fragment but not the FER^{G598E} allele (10–500 ng template DNA with an elongation temperature of 57 °C for 25 cycles). The selected double mutants were confirmed by Sanger sequencing.

Rhizosphere growth of non-tagged commensals. Rhizosphere commensal strains were grown in the rhizosphere of *fer-8* and the parental line (*pCYP71A12:GUS*). All bacterial strains were cultured in LB broth or solid LB media without antibiotics at 29 °C. *Pseudomonas* species SY10 was isolated by plating a rhizosphere sample from natural soil on King's B, selecting a fluorescent colony and streaking for single colonies. The identity as a *Pseudomonas* species was determined by amplifying the 16S rRNA with the primers 8F (5′-AGAGTTTGATCCTGGCTCAG-3′) and 1392R (5′-ACGGGCGGTGTGTRC-3′) and sequencing with the primer 8F. To quantify c.f.u. levels, *fer-8* or the parental line were grown as described above for the gnotobiotic system and bacteria were added to a final optical density measured at a wavelength of 600 nm (OD_{600}) of 0.00002 in 300 µl. The media containing bacteria surrounding plant roots was serially diluted and plated to calculate c.f.u. levels. For most of the strains, rhizosphere samples were serially diluted and plated on LB plates 2 d after inoculation, while samples of *B. phytofirmans* PsJN and *H. seropedicae* SmR1 were plated 4 d after inoculation. *P. syringae* pv. tomato DC3000 and *P. viridiflava* CH409 were plated 50–72 h after inoculation due to slow growth in the rhizosphere. The bacterial strains used in this study were described previously: *Pseudomonas* species CH267 (ref. [21]), *P. fluorescens* WCS365 (ref. [67]), *P. simiae* WCS417 (ref. [68]), *P. aeruginosa* PAO1 (ref. [69]), *P. putida* WCS358 (ref. [67]), *B. subtilis* NCIB 3610 (ref. [70]), *B. xenovorans* LB400 (ref. [71]), *H. seropedicae* SmR1 (ref. [72]), *B. phytofirmans* PsJN[73], *P. syringae* pv. tomato DC3000 (ref. [74]), *Pseudomonas* species N2C3 (ref. [75]) and *P. viridiflava* CH409 (ref. [31]). *Pseudomonas* species SY10 was identified in the natural soil used in this study.

RNA sequencing (RNA-seq) and data analysis. For RNA-seq, plants were grown on 1/2× MS with 1% phytoagar and 1% sucrose. For both the parental line (*pCYP71A12:GUS*) and *fer-8*, samples were harvested 11 d after germination. Shoots from two plants or roots from five plants were pooled for each sample. RNA was extracted using a Qiagen RNeasy isolation kit. RNA samples with a concentration higher than 300 ng µl^{-1} and an RNA integrity number (RIN) higher than eight were used for library preparation. The construction of libraries and sequencing were performed at the Michael Smith Genome Sciences Center (http://www.bcgsc.ca/). Paired-end 75-bp RNA-seq was performed using an Illumina HiSeq 2500 platform. High-quality reads were mapped to the TAIR10 genome using Bowtie 2 (ref. [76]), and transcript quantification was performed with RSEM[77]. Differential expression analysis was performed in R (https://www.R-project.org/) with the DESeq2 package[64]. Differentially expressed genes were filtered by $P_{adj} < 0.1$. Gene Ontology enrichment analysis was done using AgriGO[78]. The core jasmonic acid-responsive genes were those that were induced in response to jasmonic acid treatment at all time points from 1–16 h (a total of 12 sampling points)[79]; all other hormone-responsive genes were obtained from a previous publication[80]. The heatmap.2 function from the gplots package in R was used to generate the heatmaps.

Infection assay. The *B. cinerea* infection assays were performed as described previously[81]. Leaves 7–9 from 4-week-old plants were excised and placed adaxial side down onto 1% agar plates for infection. Then, 6 µl with 5×10^5 spores per ml was dropped onto the abaxial leaf surface. Lesion diameters were measured 3 d after inoculation.

For *P. syringae* pv. tomato DC3000 and *Pseudomonas* species N2C3 inoculation in soil, 6-d-old *Arabidopsis* seedlings were grown on 1/2× MS agar with 1% sucrose and transferred to natural soil (1:0.5:1 natural soil:calcinated clay (Turface):perlite). Inoculation was performed 1 or 2 d after transplanting. Overnight bacterial cultures were centrifuged and washed in 10 mM $MgSO_4$ three times before being diluted to an OD_{600} of 0.5 and 0.05. Then, 1 ml bacterial inoculum at $OD_{600} = 0.5$ or 0.05 for each pot (approximately 70 g of soil mixture) was added to the soil, taking care not to touch the seedlings, to reach final concentrations of 3×10^5 and 3×10^6 c.f.u. per gram of soil, respectively. The same volume of 10 mM $MgSO_4$ was used as a buffer control. Different groups were grown side by side in the same tray, but were watered separately in different trays to avoid cross-contamination.

For *P. syringae* pv. tomato DC3000 and *Pseudomonas* species N2C3 inoculation on plates, seeds were germinated on 1/2× MS plates (without sucrose), grown for 6 d and inoculated with 5 µl bacteria ($OD_{600} = 0.05$). The same volume of 10 mM $MgSO_4$ was used as a buffer control. The plates were scanned 7 d after inoculation and the plants were weighed on the same day.

Detecting ROS in roots. ROS detection was performed using H_2DCFDA fluorescent dye. Plants were grown on 1/2× MS agar plates supplemented with 1% sucrose for 4 d. Roots were inoculated with 3 µl buffer (10 mM $MgSO_4$) or *P. fluorescens* WCS365 ($OD_{600} = 0.01$), and seedlings were imaged 24 h after inoculation. H_2DCFDA was dissolved in dimethyl sulfoxide (10 mg ml^{-1}), then diluted to a 500-mM stock (10×) in 0.1 M PB buffer (pH 7.0) and stored at −20 °C. Before use, H_2DCFDA aliquots were thawed in the dark, stored on ice and diluted to a 1× working concentration in 2 ml 1/2× MS media with 0.1% 2-(*N*-morpholino) ethanesulfonic acid sodium salt. Whole seedlings were transferred to a 12-well plate with 2 ml staining solution per well and stained for 15 min at room temperature in the dark. Imaging chambers were constructed according to a JoVE protocol[82]. Imaging chambers were moulded from poly(dimethylsiloxane) gel. A 1.5% agar pad was placed into a chamber and roots were rinsed in 1/2× MS and mounted onto the pad. Glass strips placed at both ends of the glass slide provided consistent coverslip spacing and root positioning directly against the coverslip, which allowed for consistent optical resolution and fluorescence signal during image acquisition. Confocal images were acquired with a 10×/0.40 numerical aperture objective on a Leica SP8 laser scanning confocal microscope using a white-light laser. H_2DCFDA was excited with a 504-nm laser and a HyD detector was used to capture emissions between 511 and 611 nm, with the detection time gated at 0.3–12 ns to reduce autofluorescence. To ensure that all H_2DCFDA-emitted fluorescence above the background was captured, large three-dimensional image stacks (with a depth of ~120–150 µm) were taken at 2.408-µm steps (to a total of 50–60 images per root). Images were converted to .tiff files using FIJI[83] and the root area was traced manually. The H_2DCFDA signal density was quantified based on two-dimensional maximum-intensity image projections in FIJI and the total intensity was divided by the root area.

For H_2DCFDA signal detection in *fer-8* ROP2OX lines (Fig. 5g), 4-d-old seedlings (grown on 1/2× MS agar supplemented with 1% sucrose) were stained in a H_2DCFDA solution, as described above. Seedlings were transferred onto new 1/2× MS agar plates for imaging. A Leica M205FA fluorescence stereo microscope equipped with a Leica PLAN APO 2.0× CORR objective was used for high-throughput imaging of two to four seedlings per image. Images were acquired with a green fluorescent protein filter set (excitation filter = ET470/40 nm; emission filter = ET525/50 nm) at a 2- or 5-s exposure time per experiment. The fluorescence signal intensity along the first ~2 mm from the root tip was quantified using FUJI, and the background was averaged and subtracted for each image.

Statistics and data processing. Student's *t*-tests (two sided) were used to compare the statistical significance between pairs of samples. Analysis of variance (ANOVA) and Tukey's honest significant difference (HSD) test were used to determine the statistical significance during multiple comparisons using R (www.r-project.org). For c.f.u., data were found to be normal after log transformation. All statistics were performed on log-transformed data.

To compare the significance of the difference of gene expression between the parental line and *fer-8* (Supplementary Fig. 7), we first computed the average relative expression between two replicates and ranked all of the genes according to this variable within *fer-8* and the parental line. For genes from each hormone pathway, we performed normal bootstrapping on 5,000 replicates, then calculated the mean sign of differential expression of all of the genes within a given hormone pathway (if expression of a gene was higher, the same or lower in *fer-8* relative to the parental line, the sign would be 1, 0 or −1, respectively). We asked whether genes from a pathway were more likely to be upregulated in *fer-8* compared with the parental line—the null hypothesis being an average sign difference of zero. *P* values were calculated based on the normal distribution of mean signs from the 5,000 bootstrap replicates for each pathway. This procedure was applied independently for the root and shoot samples. The relative H_2DCFDA values in Fig. 5g were calculated by normalizing raw values to the average of Col-0 from the respective independent experiment.

Reporting Summary. Further information on research design is available in the Nature Research Reporting Summary linked to this article.

Data availability

The microbiome sequencing data have been deposited in the National Center for Biotechnology Information BioProject database under accession PRJNA559927. The RNA-seq raw sequencing and analysed data have been deposited in the National Center for Biotechnology Information Gene Expression Omnibus database under accession GSE167143.

Code availability

The code related to microbiome sequencing and RNA-seq analysis is available from the Haney laboratory GitHub repository (https://github.com/haneylab/).

Received: 15 January 2021; Accepted: 1 April 2021;
Published online: 10 May 2021

References

1. Rosenberg, E. & Zilber-Rosenberg, I. Microbes drive evolution of animals and plants: the hologenome concept. *mBio* **7**, e01395 (2016).
2. Lugtenberg, B. & Kamilova, F. Plant-growth-promoting rhizobacteria. *Annu. Rev. Microbiol.* **63**, 541–556 (2009).

3. Zhang, J. et al. NRT1.1B is associated with root microbiota composition and nitrogen use in field-grown rice. *Nat. Biotechnol.* **37**, 676–684 (2019).
4. Kwak, M. J. et al. Rhizosphere microbiome structure alters to enable wilt resistance in tomato. *Nat. Biotechnol.* **36**, 1100–1109 (2018).
5. Dimkpa, C., Weinand, T. & Asch, F. Plant–rhizobacteria interactions alleviate abiotic stress conditions. *Plant Cell Environ.* **32**, 1682–1694 (2009).
6. Abdelaziz, M. E. et al. *Piriformospora indica* alters Na^+/K^+ homeostasis, antioxidant enzymes and LeNHX1 expression of greenhouse tomato grown under salt stress. *Sci. Hortic.* **256**, 108532 (2019).
7. Chen, T. et al. A plant genetic network for preventing dysbiosis in the phyllosphere. *Nature* **580**, 653–657 (2020).
8. Levy, M., Kolodziejczyk, A. A., Thaiss, C. A. & Elinav, E. Dysbiosis and the immune system. *Nat. Rev. Immunol.* **17**, 219–232 (2017).
9. Berendsen, R. L. et al. Disease-induced assemblage of a plant-beneficial bacterial consortium. *ISME J.* **12**, 1496–1507 (2018).
10. Mendes, R. et al. Deciphering the rhizosphere microbiome for disease-suppressive bacteria. *Science* **332**, 1097–1100 (2011).
11. Berendsen, R. L., Pieterse, C. M. & Bakker, P. A. The rhizosphere microbiome and plant health. *Trends Plant Sci.* **17**, 478–486 (2012).
12. Vurukonda, S. S., Vardharajula, S., Shrivastava, M. & SkZ,A. Enhancement of drought stress tolerance in crops by plant growth promoting rhizobacteria. *Microbiol. Res.* **184**, 13–24 (2016).
13. Haas, D. & Defago, G. Biological control of soil-borne pathogens by fluorescent pseudomonads. *Nat. Rev. Microbiol.* **3**, 307–319 (2005).
14. Bakker, P. A., Pieterse, C. M. & van Loon, L. C. Induced systemic resistance by fluorescent *Pseudomonas* spp. *Phytopathology* **97**, 239–243 (2007).
15. Weller, D. M., Howie, W. J. & Cook, R. J. Relationship between in vitro inhibition of *Gaeumannomyces graminis* var. *tritici* and suppression of take-all of wheat by fluorescent pseudomonads. *Phytopathology* **78**, 1094–1100 (1988).
16. Mazurier, S., Corberand, T., Lemanceau, P. & Raaijmakers, J. M. Phenazine antibiotics produced by fluorescent pseudomonads contribute to natural soil suppressiveness to *Fusarium* wilt. *ISME J.* **3**, 977–991 (2009).
17. Stutz, E., Défago, G. & Kern, H. Naturally occurring fluorescent pseudomonads involved in suppression of black root rot of tobacco. *Phytopathology* **76**, 181–185 (1986).
18. Shipton, P. Monoculture and soilborne plant pathogens. *Annu. Rev. Phytopathol.* **15**, 387–407 (1977).
19. Simon, A. & Sivasithamparam, K. Pathogen-suppression: a case study in biological suppression of *Gaeumannomyces graminis* var. *tritici* in soil. *Soil Biol. Biochem.* **21**, 331–337 (1989).
20. Cook, R. J. The influence of rotation crops on take-all decline phenomenon. *Phytopathology* **71**, 189–192 (1981).
21. Haney, C. H., Samuel, B. S., Bush, J. & Ausubel, F. M. Associations with rhizosphere bacteria can confer an adaptive advantage to plants. *Nat. Plants* **1**, 15051 (2015).
22. Zhang, X. C., Millet, Y. A., Cheng, Z., Bush, J. & Ausubel, F. M. Jasmonate signalling in *Arabidopsis* involves SGT1b–HSP70–HSP90 chaperone complexes. *Nat. Plants* **1**, 15049 (2015).
23. Johnsen, K. & Nielsen, P. Diversity of *Pseudomonas* strains isolated with King's B and Gould's S1 agar determined by repetitive extragenic palindromic-polymerase chain reaction, 16S rDNA sequencing and Fourier transform infrared spectroscopy characterisation. *FEMS Microbiol. Lett.* **173**, 155–162 (1999).
24. Noguchi, T. et al. Brassinosteroid-insensitive dwarf mutants of *Arabidopsis* accumulate brassinosteroids. *Plant Physiol.* **121**, 743–752 (1999).
25. Eng, R. C. & Wasteneys, G. O. The microtubule plus-end tracking protein ARMADILLO-REPEAT KINESIN1 promotes microtubule catastrophe in *Arabidopsis*. *Plant Cell* **26**, 3372–3386 (2014).
26. Guo, H. et al. FERONIA receptor kinase contributes to plant immunity by suppressing jasmonic acid signaling in *Arabidopsis thaliana*. *Curr. Biol.* **28**, 3316–3324.e6 (2018).
27. Haruta, M., Sabat, G., Stecker, K., Minkoff, B. B. & Sussman, M. R. A peptide hormone and its receptor protein kinase regulate plant cell expansion. *Science* **343**, 408–411 (2014).
28. Duan, Q., Kita, D., Li, C., Cheung, A. Y. & Wu, H. M. FERONIA receptor-like kinase regulates RHO GTPase signaling of root hair development. *Proc. Natl Acad. Sci. USA* **107**, 17821–17826 (2010).
29. Kim, B. R. et al. Deciphering diversity indices for a better understanding of microbial communities. *J. Microbiol. Biotechnol.* **27**, 2089–2093 (2017).
30. Melnyk, R. A., Hossain, S. S. & Haney, C. H. Convergent gain and loss of genomic islands drive lifestyle changes in plant-associated *Pseudomonas*. *ISME J.* **13**, 1575–1588 (2019).
31. Haney, C. H. et al. Rhizosphere-associated *Pseudomonas* induce systemic resistance to herbivores at the cost of susceptibility to bacterial pathogens. *Mol. Ecol.* **27**, 1833–1847 (2018).
32. Carrion, V. J. et al. Pathogen-induced activation of disease-suppressive functions in the endophytic root microbiome. *Science* **366**, 606–612 (2019).
33. Raaijmakers, J. M. et al. Dose–response relationships in biological control of *Fusarium* wilt of radish by *Pseudomonas* spp. *Phytopathology* **85**, 1075–1080 (1995).
34. Ellis, C. & Turner, J. G. A conditionally fertile *coi1* allele indicates cross-talk between plant hormone signalling pathways in *Arabidopsis thaliana* seeds and young seedlings. *Planta* **215**, 549–556 (2002).
35. Zhao, C. et al. The LRXs–RALFs–FER module controls plant growth and salt stress responses by modulating multiple plant hormones. *Natl Sci. Rev.* **8**, nwaa149 (2021).
36. Spoel, S. H. et al. NPR1 modulates cross-talk between salicylate- and jasmonate-dependent defense pathways through a novel function in the cytosol. *Plant Cell* **15**, 760–770 (2003).
37. Cao, H., Bowling, S. A., Gordon, A. S. & Dong, X. Characterization of an *Arabidopsis* mutant that is nonresponsive to inducers of systemic acquired resistance. *Plant Cell* **6**, 1583–1592 (1994).
38. Dewdney, J. et al. Three unique mutants of *Arabidopsis* identify EDS loci required for limiting growth of a biotrophic fungal pathogen. *Plant J.* **24**, 205–218 (2000).
39. Zhang, Y., Goritschnig, S., Dong, X. & Li, X. A gain-of-function mutation in a plant disease resistance gene leads to constitutive activation of downstream signal transduction pathways in *suppressor of npr1-1, constitutive 1*. *Plant Cell* **15**, 2636–2646 (2003).
40. Stegmann, M. et al. The receptor kinase FER is a RALF-regulated scaffold controlling plant immune signaling. *Science* **355**, 287–289 (2017).
41. Miller, G. et al. The plant NADPH oxidase RBOHD mediates rapid systemic signaling in response to diverse stimuli. *Sci. Signal.* **2**, ra45 (2009).
42. Roux, M. et al. The *Arabidopsis* leucine-rich repeat receptor-like kinases BAK1/SERK3 and BKK1/SERK4 are required for innate immunity to hemibiotrophic and biotrophic pathogens. *Plant Cell* **23**, 2440–2455 (2011).
43. Schwessinger, B. et al. Phosphorylation-dependent differential regulation of plant growth, cell death, and innate immunity by the regulatory receptor-like kinase BAK1. *PLoS Genet.* **7**, e1002046 (2011).
44. Zhao, C. et al. Leucine-rich repeat extensin proteins regulate plant salt tolerance in *Arabidopsis*. *Proc. Natl Acad. Sci. USA* **115**, 13123–13128 (2018).
45. Xiao, Y. et al. Mechanisms of RALF peptide perception by a heterotypic receptor complex. *Nature* **572**, 270–274 (2019).
46. Masachis, S. et al. A fungal pathogen secretes plant alkalinizing peptides to increase infection. *Nat. Microbiol.* **1**, 16043 (2016).
47. Zhang, X. et al. Nematode-encoded RALF peptide mimics facilitate parasitism of plants through the FERONIA receptor kinase. *Mol. Plant* **13.10**, 1434–1454 (2020).
48. Thynne, E. et al. Fungal phytopathogens encode functional homologues of plant rapid alkalinization factor (RALF) peptides. *Mol. Plant Pathol.* **18**, 811–824 (2017).
49. Hussain, M. et al. Bacterial community assemblages in the rhizosphere soil, root endosphere and cyst of soybean cyst nematode-suppressive soil challenged with nematodes. *FEMS Microbiol. Ecol.* **94**, fiy142 (2018).
50. Huang, A. C. et al. A specialized metabolic network selectively modulates *Arabidopsis* root microbiota. *Science* **364**, eaau6389 (2019).
51. Stringlis, I. A. et al. MYB72-dependent coumarin exudation shapes root microbiome assembly to promote plant health. *Proc. Natl Acad. Sci. USA* **115**, E5213–E5222 (2018).
52. Zhou, F. et al. Co-incidence of damage and microbial patterns controls localized immune responses in roots. *Cell* **180**, 440–453 (2020).
53. Yu, K. et al. Rhizosphere-associated *Pseudomonas* suppress local root immune responses by gluconic acid-mediated lowering of environmental pH. *Curr. Biol.* **29**, 3913–3920 (2019).
54. Zhang, X., Yang, Z., Wu, D. & Yu, F. RALF–FERONIA signaling: linking plant immune response with cell growth. *Plant Commun.* **1**, 100084 (2020).
55. Campbell, L. & Turner, S. R. A comprehensive analysis of RALF proteins in green plants suggests there are two distinct functional groups. *Front. Plant Sci.* **8**, 37 (2017).
56. Gómez-Gómez, L. & Boller, T. FLS2: an LRR receptor-like kinase involved in the perception of the bacterial elicitor flagellin in *Arabidopsis*. *Mol. Cell* **5**, 1003–1011 (2000).
57. Zipfel, C. et al. Perception of the bacterial PAMP EF-Tu by the receptor EFR restricts *Agrobacterium*-mediated transformation. *Cell* **125**, 749–760 (2006).
58. Dobon, A. et al. Novel disease susceptibility factors for fungal necrotrophic pathogens in *Arabidopsis*. *PLoS Pathog.* **11**, e1004800 (2015).
59. Lane, M. C., Alteri, C. J., Smith, S. N. & Mobley, H. L. Expression of flagella is coincident with uropathogenic *Escherichia coli* ascension to the upper urinary tract. *Proc. Natl Acad. Sci. USA* **104**, 16669–16674 (2007).
60. James, G. V. et al. User guide for mapping-by-sequencing in *Arabidopsis*. *Genome Biol.* **14**, R61 (2013).
61. Li, H. & Durbin, R. Fast and accurate short read alignment with Burrows–Wheeler transform. *Bioinformatics* **25**, 1754–1760 (2009).
62. Thompson, L. R. et al. A communal catalogue reveals Earth's multiscale microbial diversity. *Nature* **551**, 457–463 (2017).

63. Callahan, B. J. et al. DADA2: high-resolution sample inference from Illumina amplicon data. *Nat. Methods* **13**, 581–583 (2016).
64. Love, M. I., Huber, W. & Anders, S. Moderated estimation of fold change and dispersion for RNA-seq data with DESeq2. *Genome Biol.* **15**, 550 (2014).
65. Ding, Y. et al. Opposite roles of salicylic acid receptors NPR1 and NPR3/NPR4 in transcriptional regulation of plant immunity. *Cell* **173**, 1454–1467 (2018).
66. Drenkard, E. et al. A simple procedure for the analysis of single nucleotide polymorphisms facilitates map-based cloning in *Arabidopsis*. *Plant Physiol.* **124**, 1483–1492 (2000).
67. Geels, F. & Schippers, B. Selection of antagonistic fluorescent *Pseudomonas* spp. and their root colonization and persistence following treatment of seed potatoes. *J. Phytopathol.* **108**, 193–206 (1983).
68. Lamers, J., Schippers, B. & Geels, F. Soil-borne diseases of wheat in the Netherlands and results of seed bacterization with pseudomonads against *Gaeumannomyces graminis* var. *tritici*, associated with disease resistance. In *Cereal Breeding Related to Integrated Cereal Production: Proceedings of the Conference of the Cereal Section of EUCARPIA* 134–139 (European Association for Research on Plant Breeding, 1988).
69. Holloway, B. W. Genetic recombination in *Pseudomonas aeruginosa*. *J. Gen. Microbiol.* **13**, 572–581 (1955).
70. Branda, S. S., Gonzalez-Pastor, J. E., Ben-Yehuda, S., Losick, R. & Kolter, R. Fruiting body formation by *Bacillus subtilis*. *Proc. Natl Acad. Sci. USA* **98**, 11621–11626 (2001).
71. Denef, V. J. et al. Biphenyl and benzoate metabolism in a genomic context: outlining genome-wide metabolic networks in *Burkholderia xenovorans* LB400. *Appl. Environ. Microbiol.* **70.8**, 4961–4970 (2004).
72. Baldani, J., Baldani, V., Seldin, L. & Döbereiner, J. Characterization of *Herbaspirillum seropedicae* gen. nov., sp. nov., a root-associated nitrogen-fixing bacterium. *Int. J. System. Evol. Microbiol.* **36**, 86–93 (1986).
73. Sawana, A., Adeolu, M. & Gupta, R. S. Molecular signatures and phylogenomic analysis of the genus *Burkholderia*: proposal for division of this genus into the emended genus *Burkholderia* containing pathogenic organisms and a new genus *Paraburkholderia* gen. nov. harboring environmental species. *Front. Genet.* **5**, 429 (2014).
74. Cuppels, D. A. Generation and characterization of Tn5 insertion mutations in *Pseudomonas syringae* pv. *tomato*. *Appl. Environ. Microbiol.* **51**, 323–327 (1986).
75. Price, M. N. et al. Mutant phenotypes for thousands of bacterial genes of unknown function. *Nature* **557**, 503–509 (2018).
76. Langmead, B., Trapnell, C., Pop, M. & Salzberg, S. L. Ultrafast and memory-efficient alignment of short DNA sequences to the human genome. *Genome Biol.* **10**, R25 (2009).
77. Li, B. & Dewey, C. N. RSEM: accurate transcript quantification from RNA-seq data with or without a reference genome. *BMC Bioinform.* **12**, 323 (2011).
78. Tian, T. et al. agriGO v2.0: a GO analysis toolkit for the agricultural community, 2017 update. *Nucleic Acids Res.* **45**, W122–W129 (2017).
79. Hickman, R. et al. Architecture and dynamics of the jasmonic acid gene regulatory network. *Plant Cell* **29**, 2086–2105 (2017).
80. Nemhauser, J. L., Hong, F. & Chory, J. Different plant hormones regulate similar processes through largely nonoverlapping transcriptional responses. *Cell* **126**, 467–475 (2006).
81. Genenncher, B. et al. Nucleoporin-regulated MAP kinase signaling in immunity to a necrotrophic fungal pathogen. *Plant Physiol.* **172**, 1293–1305 (2016).
82. Kirchhelle, C. & Moore, I.A simple chamber for long-term confocal imaging of root and hypocotyl development. *J. Vis. Exp.* **2017**, e55331 (2017).
83. Schindelin, J. et al. Fiji: an open-source platform for biological-image analysis. *Nat. Methods* **9**, 676–682 (2012).

Acknowledgements

We thank F. M. Ausubel for critical reading of the manuscript and generous provision of the *hsm* mutant collection; A. Y. Cheung, Z. Y. Wang, X. Li, Y. Zhang and G. Wasteneys for kindly providing seed stocks; and the laboratory of M. Hirst for assistance with sequencing. This work was supported by an NSERC Discovery Grant (NSERC-RGPIN-2016-04121) and Weston Seeding Food Innovation grants awarded to C.H.H. Y.S. was supported by a kick-start award from the Michael Smith Laboratories (UBC) and a fellowship from the Chinese Postdoctoral Science Foundation. Early stages of this work were supported by NIH R37 grant GM48707 and NSF grants MCB-0519898 and IOS-0929226 awarded to F. Ausubel.

Author contributions

C.H.H. and Y.S. conceived of the project and designed the experiments. Y.S. performed the majority of experiments and data analysis. X.-C.Z. performed the previous *hsm* screen. A.J.W. analysed the RNA-seq and microbiome profiling data. D.T. conducted the confocal microscopy imaging. Q.G. performed statistical analysis for the expression of hormone-responsive genes and Pearson correlation assays. S.S., Y.L. and L.W. helped with the gnotobiotic plant assays. Experiments related to *mfec* were performed by R.S. with input from S.Y.H. C.H.H. and Y.S. wrote the manuscript with input from all authors.

Competing interests

The authors declare no competing interests.

Additional information

Supplementary information The online version contains supplementary material available at https://doi.org/10.1038/s41477-021-00914-0.

Correspondence and requests for materials should be addressed to C.H.H.

Peer review information *Nature Plants* thanks the anonymous reviewers for their contribution to the peer review of this work.

Reprints and permissions information is available at www.nature.com/reprints.

Publisher's note Springer Nature remains neutral with regard to jurisdictional claims in published maps and institutional affiliations.

nature research

Corresponding author(s): Cara H. Haney

Last updated by author(s): 3/23/2021

Reporting Summary

Nature Research wishes to improve the reproducibility of the work that we publish. This form provides structure for consistency and transparency in reporting. For further information on Nature Research policies, see our Editorial Policies and the Editorial Policy Checklist.

Statistics

For all statistical analyses, confirm that the following items are present in the figure legend, table legend, main text, or Methods section.

n/a	Confirmed	
☐	☒	The exact sample size (*n*) for each experimental group/condition, given as a discrete number and unit of measurement
☐	☒	A statement on whether measurements were taken from distinct samples or whether the same sample was measured repeatedly
☐	☒	The statistical test(s) used AND whether they are one- or two-sided *Only common tests should be described solely by name; describe more complex techniques in the Methods section.*
☒	☐	A description of all covariates tested
☐	☒	A description of any assumptions or corrections, such as tests of normality and adjustment for multiple comparisons
☐	☒	A full description of the statistical parameters including central tendency (e.g. means) or other basic estimates (e.g. regression coefficient) AND variation (e.g. standard deviation) or associated estimates of uncertainty (e.g. confidence intervals)
☐	☒	For null hypothesis testing, the test statistic (e.g. *F*, *t*, *r*) with confidence intervals, effect sizes, degrees of freedom and *P* value noted *Give P values as exact values whenever suitable.*
☒	☐	For Bayesian analysis, information on the choice of priors and Markov chain Monte Carlo settings
☒	☐	For hierarchical and complex designs, identification of the appropriate level for tests and full reporting of outcomes
☐	☒	Estimates of effect sizes (e.g. Cohen's *d*, Pearson's *r*), indicating how they were calculated

Our web collection on statistics for biologists contains articles on many of the points above.

Software and code

Policy information about availability of computer code

Data collection	No software was used for data collection
Data analysis	R version 4.0.0, Excel: Microsoft Office Professional Plus 2016; graphpad prism 7; DADA2; and QIIME2 were used for data analysis and referenced in the manuscript. Additional code for 16S rRNA analysis in R will be made available at https://github.com/haneylab/.

For manuscripts utilizing custom algorithms or software that are central to the research but not yet described in published literature, software must be made available to editors and reviewers. We strongly encourage code deposition in a community repository (e.g. GitHub). See the Nature Research guidelines for submitting code & software for further information.

Data

Policy information about availability of data

All manuscripts must include a data availability statement. This statement should provide the following information, where applicable:

- Accession codes, unique identifiers, or web links for publicly available datasets
- A list of figures that have associated raw data
- A description of any restrictions on data availability

The microbiome sequencing data was deposited in NCBI under PRJNA559927, and RNAseq raw sequencing data and analysis will be available at NCBI under GSE167143 after publication.

Field-specific reporting

Please select the one below that is the best fit for your research. If you are not sure, read the appropriate sections before making your selection.

☒ Life sciences ☐ Behavioural & social sciences ☐ Ecological, evolutionary & environmental sciences

For a reference copy of the document with all sections, see nature.com/documents/nr-reporting-summary-flat.pdf

Life sciences study design

All studies must disclose on these points even when the disclosure is negative.

Sample size	No sample size calculations were performed. Sample sizes were determined empirically based on past use of similar assays by our lab (i.e. hydroponic assay), or descriptions of appropriate samples sizes in the literature (i.e. 16S rRNA sequencing).
Data exclusions	For the hydroponic assay, plants with translucent leaves were discarded from analysis. This is described in the methods.
Replication	All experiments were replicated at least 2 additional times (at least 3 total independent experiments) with the exception of the soil transplant experiment (Figure 3) that was performed 2 independent times. Details of replication are described in the methods and figure legends.
Randomization	For 16S rRNA experiments and other microbiome experiments, plant genotypes were randomized within trays.
Blinding	The experiments were not blinded.

Reporting for specific materials, systems and methods

We require information from authors about some types of materials, experimental systems and methods used in many studies. Here, indicate whether each material, system or method listed is relevant to your study. If you are not sure if a list item applies to your research, read the appropriate section before selecting a response.

Materials & experimental systems

n/a	Involved in the study
☒	☐ Antibodies
☒	☐ Eukaryotic cell lines
☒	☐ Palaeontology and archaeology
☒	☐ Animals and other organisms
☒	☐ Human research participants
☒	☐ Clinical data
☒	☐ Dual use research of concern

Methods

n/a	Involved in the study
☒	☐ ChIP-seq
☒	☐ Flow cytometry
☒	☐ MRI-based neuroimaging